https://dx.doi.org/10.1016/j.jlumin.2023.120069

Efficient blue and deep blue fluorescent OLEDs based on anthracene with upper-level intersystem crossing

Minting Ouyang [a, b], Runda Guo [c], He Jiang [a, b], Lei Wang [c]*, Wai-Yeung Wong [a, b]*

[a] *Department of Applied Biology and Chemical Technology and Research Institute for Smart Energy, The Hong Kong Polytechnic University (PolyU), Hung Hom, Hong Kong, P. R. China*

[b] *PolyU Shenzhen Research Institute, Shenzhen 518057, P.R. China*

[c] *Wuhan National Laboratory for Optoelectronics, Huazhong University of Science and Technology, Wuhan 430074, P.R. China*

Keywords: Anthracene, Deep blue emission, Hot exciton, Hybridized local and charge-transfer (HLCT), Organic light-emitting diode (OLED)

Abstract

Two new emitters based on anthracene core, 6-(10-phenylanthracen-9-yl)nicotinonitrile (CNPyAnPh) and 4-(10-(pyridin-2-yl)anthracen-9-yl)benzonitrile (CNPhAnPy) are designed and synthesized for realizing blue and deep blue organic light-emitting diodes (OLEDs). Both CNPyAnPh and CNPhAnPy show nearly orthogonal structures and the suppressed π-conjugation is favorable for blue and even deep blue emission. According to the theoretical calculations, small energy differences between T_2 and S_1 are observed in these two isomers, endowing the "hot exciton" channel. Furthermore, the S_1 of CNPyAnPh possesses both locally excited (LE) and charge transfer (CT) components. By employing CNPyAnPh and CNPhAnPy as the emissive guests in the devices, their maximum external quantum efficiencies (EQE_{max}s)

are 4.15% and 3.71%, respectively. Thanks to the “hot exciton” and hybrid local and charge transfer (HLCT) properties, the exciton utilization efficiencies (EUEs) of two molecules are higher than 25%, 42% for CNPyAnPh and 34% for CNPhAnPy. The Commission International de l’Eclairage (CIE) coordinate of CNPhAnPy is (0.15, 0.08), approaching the National Television System Committee (NTSC) standard index for pure blue emission.

1. Introduction

In the 1980s, the first sandwich-like organic light-emitting diode (OLED), which can be driven by a relatively low voltage, was reported by Tang and coworkers[1]. After three decades of development, OLEDs have attracted wide attention for their potential in applying to flat panel displays and solid-state lighting. As for the three primary colors of OLED displays, highly efficient blue emitters are still in great demand, compared with the red and green ones[2-4]. External quantum efficiency (EQE) is one of the important parameters to evaluate the performance of OLED devices. It can be described by the equation: $\eta_{EQE} = \gamma \bullet \phi_{PL} \bullet \eta_{S/T} \bullet \eta_{out}$, in which γ is the charge balance factor (assuming $\gamma = 1$); ϕ_{PL} is the photoluminescent quantum efficiency (PLQY) of the emitter; $\eta_{S/T}$ is the exciton utilization efficiency (EUE); η_{out} is the outcoupling efficiency ($\approx$ 0.2)[5-7]. Driven by the electric field, hole/electron pairs, namely excitons, will form in the emissive layer. Based on the spin statistics, the ratio of singlet excitons and their triplet counterparts is 1:3[8-11]. For the conventional fluorophores, their internal quantum efficiency (IQE) is limited to only 25%, and the decay of triplet excitons is nonradiative. To break through this limitation, Forrest’s group reported an OLED

device based on the phosphorescent emitter, of which the theoretical IQE can achieve 100% *via* introducing the noble metal to the emitter[12]. Still, the introduction of noble metals will cause high cost. Therefore, thermally activated delayed fluorescent (TADF) materials and fluorophores with hot exciton pathways are intensively developed[6].

TADF and "hot exciton" can utilize triplet excitons through the reverse intersystem crossing (RISC) process and high-lying RISC (hRISC) pathway, respectively, without using noble metals[13-20]. In general, the lowest singlet state (S_1) and the lowest triplet state (T_1) of TADF emitters are the charge transfer states because the highest occupied molecular orbitals (HOMOs) and the lowest unoccupied molecular orbitals (LUMOs) need to be highly separated to achieve a small energy difference between S_1 and T_1 (ΔE_{ST}) for efficient RISC process. The strong intramolecular charge transfer (ICT) from donors (D) to acceptors (A) leads to a significant Stokes shift, which makes it relatively difficult to construct deep blue TADF emitters (Commission International de l'Eclairage CIEy<0.1)[21]. Moreover, the RISC process between S_1 and T_1 is slower than the radiative process from S_1 to S_0, resulting in the quenching of triplet excitons and thus undesirable efficiency roll-off for the TADF-based OLED devices[22, 23]. On the other hand, "hot exciton" fluorophores realize hRISC from the high-lying triplet state (T_m, $m \geqslant 2$) to the singlet state (S_n, $n \geqslant 1$)[24, 25]. The hRISC process happens within several nanoseconds, which is fast and can effectively improve the device stability[16, 26]. In addition, there is a significant energy difference between T_1 and T_2, which can prevent the loss of T_m excitons caused by the internal conversion (IC) from T_2 to T_1[27, 28]. Recent studies found that hybrid local and charge transfer (HLCT)

chromophores possess the “hot exciton” property[6]. Materials with the HLCT property have both locally excited (LE) and charge transfer (CT) components, where the LE component can guarantee considerable oscillator strength (*f*) and high PLQY, and the CT counterpart can fully utilize the triplet excitons[6, 29].

Anthracene is an emissive building block with a long history. In the 1960s, organic electroluminescence (EL) was first discovered in anthracene as single crystals[30]. After that, many studies have been conducted on the anthracene core, since it is easily modified and has considerate PLQY and good carrier mobility[4, 28, 31-33]. Furthermore, the delicate alignment of anthracene's energy levels makes it possible to realize the hRISC process[34, 35]. In this work, we designed and synthesized two blue emitters based on anthracene, CNPyAnPh and CNPhAnPy (Scheme 1). Acceptors and the π conjugated unit were introduced to the 9- and 10- positions of the anthracene to further modulate the excited-state properties. The introduction of cyano and pyridine can reduce the electron injection barrier of devices because they are electron-deficient units and can lower the LUMO energy level of the emitters[36]. These two isomers possessed the “hot exciton” property and HLCT characteristics were also found in CNPyAnPh. The OLED devices based on CNPyAnPh and CNPhAnPy exhibited blue and deep blue emission with the EQE_{max} of 4.15% and 3.71%, respectively.

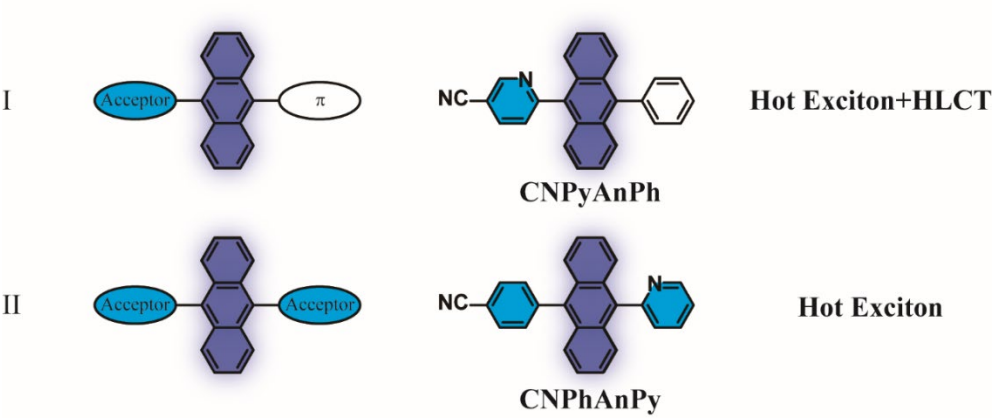

Scheme1 Chemical structures of CNPyAnPh and CNPhAnPy.

2. Results and Discussion

2.1. Synthesis and Characterization

The synthesis of CNPyAnPh and CNPhAnPy is illustrated in ESI. Firstly, 6-(anthracen-9-yl)nicotinonitrile (1) and 2-(anthracen-9-yl)pyridine (3) were synthesized through the Suzuki coupling reaction. Next, intermediate 1 and 3 were brominated with *N*-bromosuccinimide (NBS) at room temperature. Finally, bromoanthracene derivatives (2 and 4) were coupled with phenylboronic acid and 4-cyanophenylboronic acid *via* Pd-catalyzed Suzuki reaction to afford the target compounds, CNPyAnPh and CNPhAnPy, respectively. The molecular structures and the purity of the target materials were fully characterized by ^{1}H NMR, ^{13}C NMR, MALDI-TOF mass spectrometry and single-crystal X-ray diffraction.

2.2. Crystal Structures

The single crystals of CNPyAnPh (CCDC 2246065) and CNPhAnPy (CCDC 2246066) were cultivated through the slow evaporation of a mixture of dichloromethane and *n*-hexane. As shown in Figure 1a and 1c, both CNPyAnPh and CNPhAnPy exhibit nearly orthogonal configurations and these two compounds show

similar dihedral angles of 85.18° and 89.88° between neighboring cyano-containing moieties and anthracene, respectively. On the other hand, the dihedral angle between anthracene and the phenyl ring is 70.06°, smaller than the one between anthracene and pyridine, which is 84.69°. The twisted configuration can reduce the degree of the intramolecular π conjugation, which is favorable for constructing blue or even deep blue emitters. In the packing structure of CNPyAnPh and CNPhAnPy, no obvious $\pi\cdots\pi$ intermolecular interaction is observed. However, several intermolecular hydrogen bonds are found due to the introduction of the CN unit and pyridine. There is a weak C-H···N hydrogen bonding in CNPyAnPh, of which the distance is 3.834 Å. Three types of hydrogen bonds are observed in CNPhAnPy with distances ranging from 2.573 to 3.533 Å, which are relatively strong. Meanwhile, a strong C-H$\cdots\pi$ interaction is also found in the cell unit of CNPyAnPh and the corresponding distance is 2.905 Å. Those supramolecular interactions can efficiently diminish molecular motion and thus suppress the non-radiative energy loss.

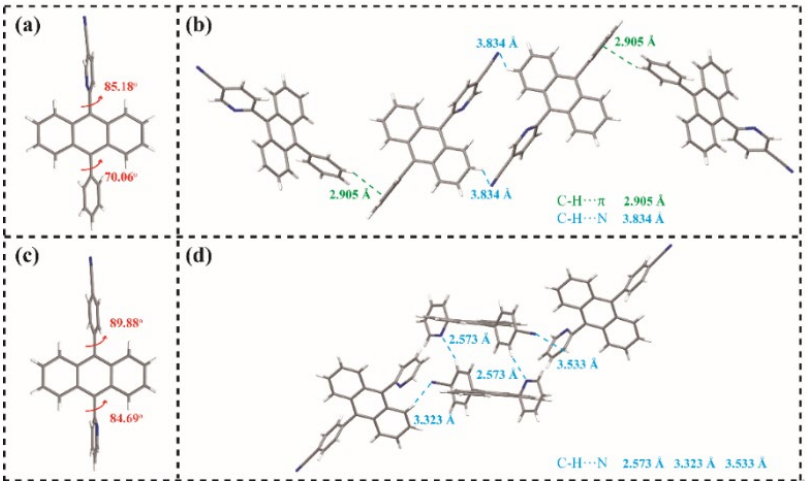

Figure 1 X-ray single crystal structures of (a) CNPyAnPh and (c) CNPhAnPy; packing patterns of (b) CNPyAnPh and (d) CNPhAnPy. The grey, blue, and white balls denote

carbon, nitrogen, and hydrogen atoms, respectively.

2.3. Theoretical Calculations

To study the electron distribution of CNPyAnPh and CNPhAnPy, the density functional theory (DFT) calculations were performed using the Gaussian 09 program package at the B3LYP/6-31G (d) basis set. As shown in Figure 2a, the distributions of frontier molecular orbitals (FMOs) of these two emitters are extremely different. The LUMO of CNPyAnPh is mainly distributed on the anthracene core and the electron-deficient cyanopyridine unit and its HOMO is mostly localized on the anthracene unit, with a residual portion on the cyanopyridine moiety, indicating the presence of both LE and CT components. In contrast, the FMOs of CNPhAnPy are fully delocalized on the anthracene core with negligible distribution on the adjacent pyridine unit, which means the LE feature dominates the electronic transition. The calculated optical energy gaps (E_g) are large enough to emit in the short wavelength region, 3.33 and 3.48 eV for CNPyAnPh and CNPhAnPy, respectively.

To get insight into the excited state characteristics of CNPyAnPh and CNPhAnPy, the natural transition orbitals (NTOs) were calculated through time-dependent DFT (TD-DFT) at the B3LYP/6-31G (d) level based on the optimized ground-state geometries. As depicted in Figures 2b and S5, the $S_0 \rightarrow S_1$, $S_0 \rightarrow S_2$ and $S_0 \rightarrow T_2$ NTOs of CNPyAnPh clearly illustrate the HLCT transition features, in which hole and particle exhibit a significant separation and a considerable degree of overlap. However, typical LE characteristics are found in $S_0 \rightarrow S_1$, $S_0 \rightarrow T_1$ and $S_0 \rightarrow T_2$ NTOs of CNPhAnPy, where hole and particle fully overlap over the anthracene core. The f of $S_0 \rightarrow S_1$ of CNPhAnPy

(0.1744) is higher than that of CNPyAnPh (0.1513), due to the LE-dominating characteristics of CNPhAnPy. The calculated energy gaps between T_2 and S_1 are 0.0103 and 0.1104 eV for CNPyAnPh and CNPhAnPy, respectively, showing a potential hRISC channel from T_2 to S_1[16, 35]. In addition, the energy differences between T_2 and T_1 are significantly large (1.1841 eV for CNPyAnPh and 1.5260 eV for CNPhAnPy), which is also one of the properties of the "hot exciton" fluorophores[37, 38].

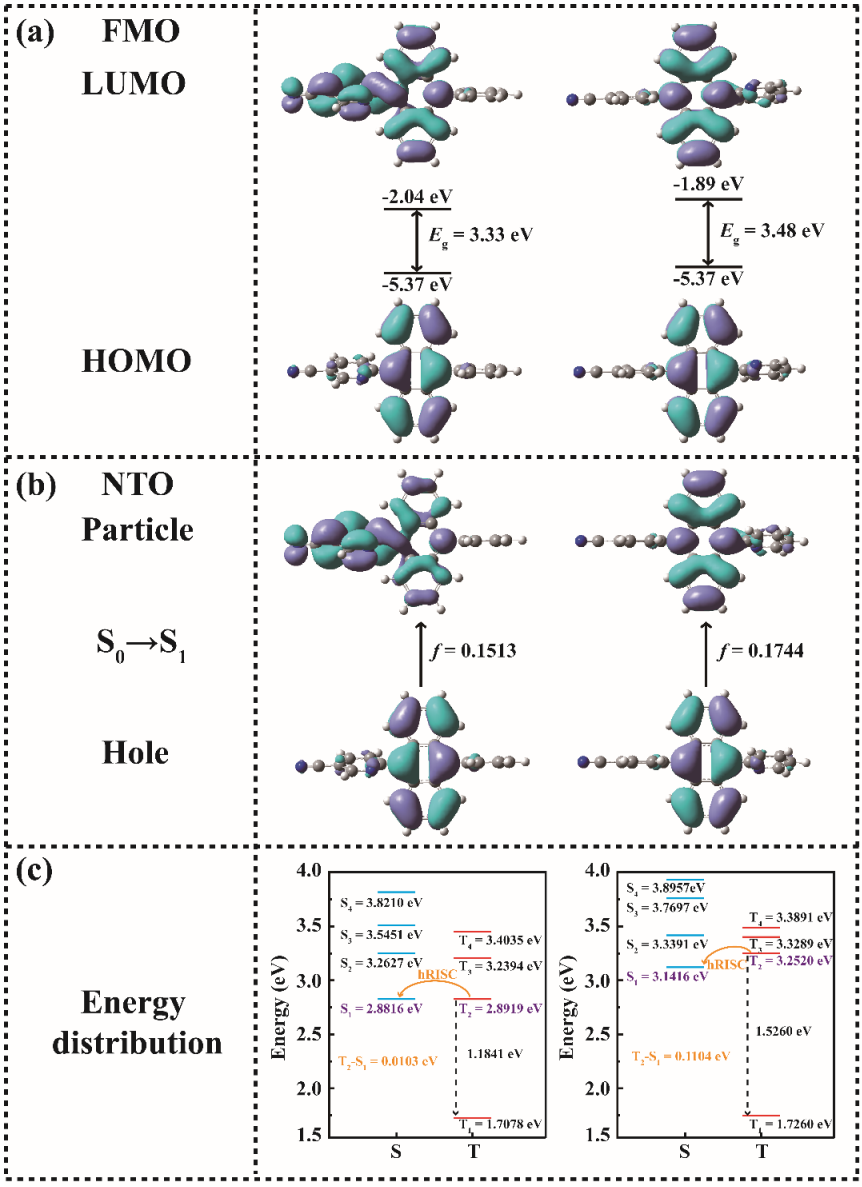

Figure 2 The (a) frontier molecular orbitals (FMOs), (b) natural transition orbitals

(NTOs) and (c) energy levels of singlet/triplet state of CNPyAnPh (left) and CNPhAnPy (right).

2.4. Photophysical Properties

The photophysical properties of these emitters are shown in Figure 3 and summarized in Table 1. From Figure 3a, the absorption bands of these two anthracene-based isomers exhibit similar profiles because of the identical skeleton. The wide absorption bands ranging from 330 to 400 nm correspond to the vibrational structure of the anthracene backbone. The photoluminescent spectra of CNPyAnPh and CNPhAnPy exhibit structureless profile and show blue and deep blue emission with the emission peaking 468 and 429 nm, respectively. To further demonstrate the properties of S_1 excited state of these two emitters, their emissions in nine types of solvents with different polarities were studied. The λ_{PL} of CNPyAnPh in *n*-hexane is 461 nm. With the increasing polarity of solvents, its emission shows a red shift of 13 nm, indicating the involvement of the CT component. In contrast, only 5 nm red shift occurs for CNPhAnPy with the increase of solvent polarity, illustrating the LE-dominated excited state. The properties of the excited states can be further confirmed by the solvatochromic Lippert-Mataga models of these two isomers. The curves of the Stokes shift (ν_a-ν_f) versus the orientation polarization (f) of solvents are shown in Figure 3d and the corresponding results are summarized in Tables S1 and S2. It is observed that the curve of CNPyAnPh can be divided into two parts, confirming the LE and CT hybrid. CNPyAnPh shows a small dipole moment in low polarity solvents ($f \leq 0.148$) and a larger dipole moment in high polarity solvents ($f \geq 0.167$). In contrast, CNPhAnPy

exhibits a small dipole moment in both low and high polarity solvents, showing a typical LE state. The result of solvatochromic Lippert-Mataga models is in good accordance with theoretical calculations. The transition PL decay curves of CNPyAnPh and CNPhAnPy show single components and short lifetimes (2.35 ns for CNPyAnPh and 0.97 ns for CNPhAnPy), implying that TADF and phosphorescent mechanism can be excluded and CNPyAnPh have LE and CT components in one HLCT excited state. In addition, the PLQYs of CNPyAnPh and CNPhAnPy are 49% and 55%, respectively.

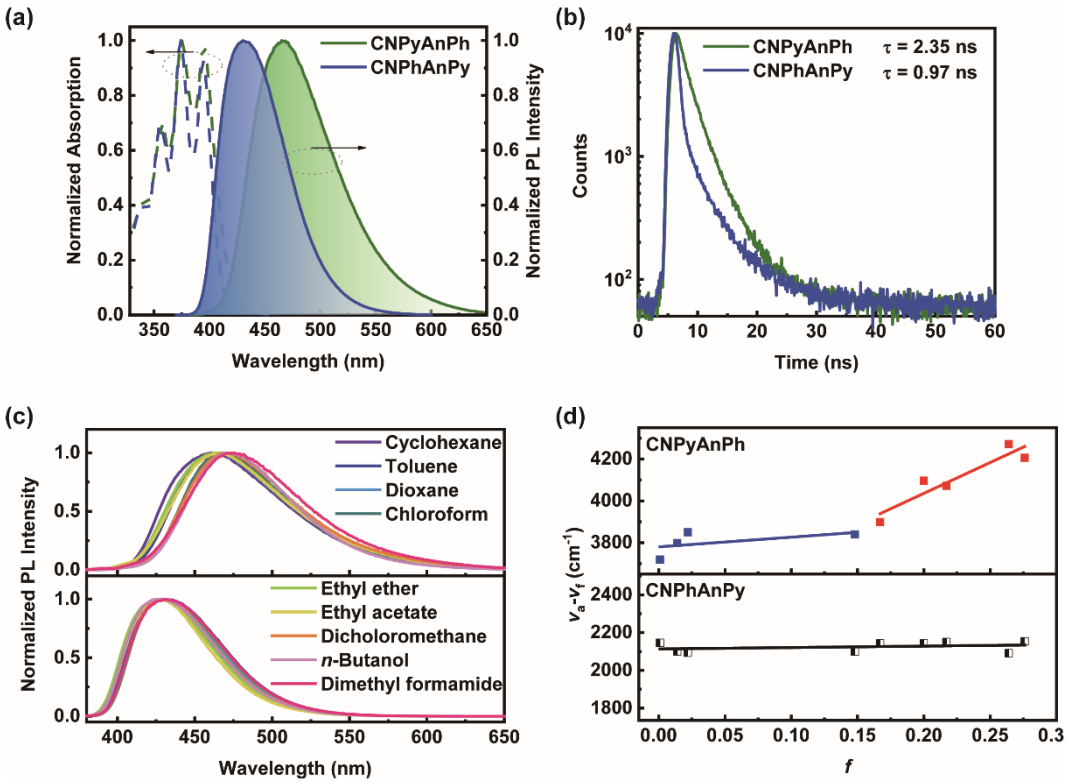

Figure 3 (a) The UV-Vis absorption and PL spectra measured in toluene (10^{-5} M, λ_{ex} = 355 nm), (b) transition PL decay spectra in the neat films (λ_{ex} = 355 nm), (c) PL spectra measured in various solvents (10^{-5} M, λ_{ex} = 370 nm) and (d) solvatochromic Lippert-Mataga models of CNPyAnPh and CNPhAnPy.

Table 1 Photophysical, thermal and electrochemical data of CNPyAnPh and

CNPhAnPy.

Compound	λ_{abs}[a] (nm)	λ_{PL}[a] (nm)	T_d[b] (°C)	HOMO[c]/LUMO[d] (eV)	E_g[e] (eV)	τ[f] (ns)	Φ[g] (%)
CNPyAnPh	352, 373, 395	468	352	-5.55/-2.60	2.95	2.35	49
CNPhAnPy	355, 373, 392	429	333	-5.54/-2.51	3.03	0.97	55

[a] Measured in toluene (10^{-5} M) at room temperature. [b] Recored at 5% weight loss. [c] Calculated from the onsets of oxidation curves. [d] Deduced from HOMO and optical energy gap. [e] Calculated by absorption cutoffs. [f] Measured in neat film at room temperature. [g] PLQY relative to 9,10-diphenylanthracene (90% in cyclohexane).

2.5. Thermal and Electrochemical Properties

The thermal stability of two isomers was characterized by thermal gravimetric analysis (TGA) and differential scanning calorimetry (DSC) (Figure S6a). The decomposition temperature of CNPyAnPh and CNPhAnPy are 352 and 333 °C, respectively. From DSC, only melting temperatures (T_m) are observed (261 °C for CNPyAnPh and 299 °C for CNPhAnPy) and no glass transition temperatures (T_g) are found for both materials.

According to the cyclic voltammetry (CV) curves, the HOMO energy levels (E_{HOMO}) of CNPyAnPh and CNPhAnPy are -5.55 and -5.54 eV, respectively. Based on E_{HOMO} and E_g, the LUMO energy values (E_{LUMO}) are deduced to be -2.60 and -2.51 eV, respectively.

2.6. Electroluminescence Properties

CNPyAnPh and CNPhAnPy were employed as emissive dopants to fabricate OLED devices to investigate their potential for electroluminescent applications. According to the photophysical and HOMO and LUMO energy levels of these two

emitters, the device structures were designed and fabricated as follows: ITO/ MoO_3 (10 nm)/ TAPC (60 nm)/ TCTA (10 nm)/ mCP: emitter (10 wt.%, 20 nm)/ TmPyPB (40 nm)/ LiF (1nm)/ Al (100 nm) (emitter = CNPyAnPh for device A and emitter = CNPhAnPy for device B), where mCP (1,3-di(9*H*-carbazol-9-yl)benzene) serves as the host. ITO (indium tin oxide), TAPC (1,1-bis[(di-4-tolylamino)phenyl]cyclohexane) and TCTA (tris(4-carbazoyl-9-ylphenyl)amine) act as the anode, hole transporting layer and exciton-blocking layer, respectively. TmPyPB (1,3,5-tris(3-pyridyl-3-phenyl) functions as the electron-transporting layer and LiF is used as the electron-injecting layer. The device performance is shown in Figure 4b-d and summarized in Table 2. As shown in the electroluminescent (EL) spectra (Figure 4b), CNPyAnPh and CNPhAnPy based OLED devices exhibit blue and deep blue emission, peaking at 468 and 448 nm, respectively. Notably, the CIE coordinates of devices A and B are (0.15, 0.18) and (0.15, 0.08) and the one for CNPhAnPy based device can approach the standard blue index of the National Television System Committee (NTSC) of (0.14, 0.08)[31, 39, 40]. The turn-on voltages (V_{on}) of devices A and B are 3.6 and 3.8 V, respectively. The maximum EQE, maximum current efficiency (CE) and maximum power efficiency (PE) are 4.15%, 6.35 cd/A and 4.34 lm/W for device A and 3.71%, 2.94 cd/A and 2.00 lm/W for device B, respectively. Based on the EQE_{max} of the devices and the PLQY of the emitters, the EUE of CNPyAnPh and CNPhAnPy based devices are calculated to be 42% and 34%, breaking through the limitation of 25%. The device performances of these two isomers are comparable among blue OLEDs based on A-An-π or A-An-A configuration by hot exciton strategy with $CIE_y \leq 0.18$ (Table S3).

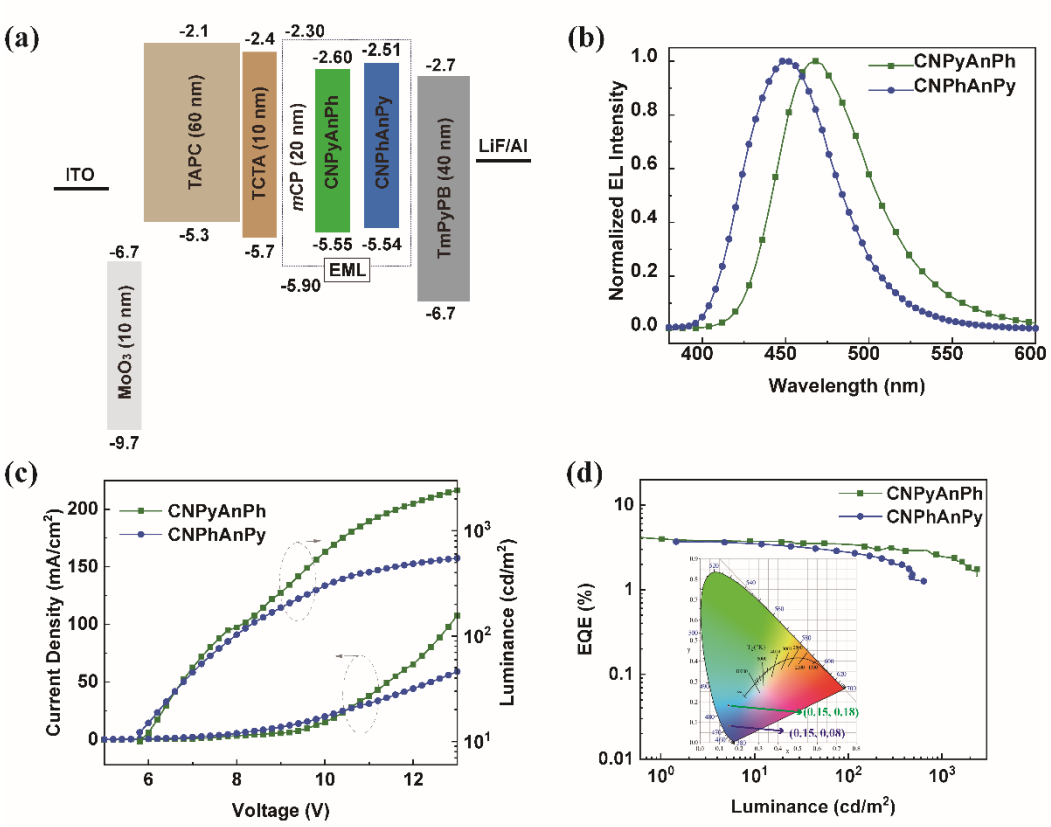

Figure 4 (a) The doped device structures of CNPyAnPh and CNPhAnPy and the corresponding energy level diagrams, (b) electroluminescent (EL) spectra, (c) current density–voltage–luminance (*J*–*V*–*L*) characteristics, and (d) EQE–luminance curves (the CIE coordinates in the inset).

Table 2 Key parameters for EL performance of device A and B.

Device	V_{on}[a] (V)	λ_{EL}[b] (nm)	CIE[b] (x,y)	CE[c] (cd/A)	PE[c] (lm/W)	EQE[c] (%)
A	3.6	468	(0.15, 0.18)	6.35	4.34	4.15
B	3.8	448	(0.15, 0.08)	2.94	2.00	3.71

[a] Measured at a luminance of 1 cd/m^2. [b] Recorded at a luminance of 100 cd/m^2 [c] Device performances recorded at maximum.

3. Conclusion

In summary, two anthracene-based emitters with “hot exciton” properties,

CNPyAnPh and CNPhAnPy, have been designed and synthesized. According to the theoretical calculations, the energy gaps between T_2 and S_1 of these two isomers are 0.0103 and 0.1104 eV, implying the potential for the "hot exciton" channel. In addition, the S_1 of CNPyAnPh shows HLCT property, which is further confirmed by its solvatochromic Lippert-Mataga model. These two emitters are employed as the emissive guest to investigate their EL properties. The device based on CNPyAnPh shows blue emission with an EQE_{max} at 4.15%. The CNPhAnPy based device affords an EQE_{max} at 3.71% with the CIE coordinates at (0.15, 0.08), close to the NTSC standard blue index. The EUEs of these two isomers break through the limitation of 25%, indicating the "hot exciton" pathway and the HLCT excited state revealed by the theoretical calculations are reasonable.

Acknowledgements

We acknowledge the National Key R&D Program of China (2022YFE0104100), ITC Guangdong-Hong Kong Technology Cooperation Funding Scheme (TCFS) (GHP/038/19GD), CAS-Croucher Funding Scheme for Joint Laboratories (ZH4A), the Hong Kong Research Grants Council (PolyU 15305320), the Hong Kong Polytechnic University, Miss Clarea Au for the Endowed Professorship in Energy (847S) and Research Institute for Smart Energy (CDAQ) for financial support. We thank Limin Zhang for help with the X-ray crystal structure analysis.

References

[1] C.W. Tang, S.A. VanSlyke, Organic electroluminescent diodes, Appl. Phys. Lett. 51 (1987) 913-915.

[2] X. He, L. Gao, H. Liu, F. Liu, D. Jiang, C. Du, C. Sun, P. Lu, Highly efficient red fluorescent OLEDs based on diphenylacridine-naphthothiadiazole derivatives with upper level intersystem crossing, Chem. Eng. J. 404 (2021) 127055.

[3] D.-D. Xie, H.-S. Liao, Y.-H. Jian, D. Chen, H.-J. Chi, B.-Y. Wang, Y.-L. Lv, Y. Dong, X. Li, Achieving high-performance non-doped sky-blue OLEDs with negligible efficiency roll-off by combining AIE, HLCT and mechanoluminescence features, Dyes Pigm. 209 (2023) 110951.

[4] S. Zeng, C. Xiao, J. Zhou, Q. Dong, Q. Li, J. Lim, H. Ma, J.Y. Lee, W. Zhu, Y. Wang, Deep blue emitter based on tris(triazolo)triazine moiety with CIE_y < 0.08 for highly efficient solution-processed organic light-emitting diodes via molecular strategy of "hot excitons", Adv. Funct. Mater. 32 (2022) 2113183.

[5] K.-H. Kim, J.-J. Kim, Origin and control of orientation of phosphorescent and TADF dyes for high-efficiency OLEDs, Adv. Mater. 30 (2018) 1705600.

[6] Y. Xu, P. Xu, D. Hu, Y. Ma, Recent progress in hot exciton materials for organic light-emitting diodes, Chem. Soc. Rev. 50 (2021) 1030-1069.

[7] D.D.C. Bradley, R.H. Friend, A.B. Holmes, T. Tsutsui, E. Aminaka, C.P. Lin, D.-U. Kim, Extended molecular design concept of molecular materials for electroluminescence: Sublimed-dye films, molecularly doped polymers and polymers with chromophores, Philos. Trans. R. Soc. A 355 (1997) 801-814.

[8] C.-H. Chen, N.T. Tierce, M.-k. Leung, T.-L. Chiu, C.-F. Lin, C.J. Bardeen, J.-H. Lee, Efficient triplet-triplet annihilation upconversion in an electroluminescence device with a fluorescent sensitizer and a triplet-diffusion singlet-blocking layer, Adv. Mater. 30 (2018) 1804850.

[9] N. Sharma, M.Y. Wong, D. Hall, E. Spuling, F. Tenopala-Carmona, A. Privitera, G. Copley, D.B. Cordes, A.M.Z. Slawin, C. Murawski, M.C. Gather, D. Beljonne, Y. Olivier, I.D.W. Samuel, E. Zysman-Colman, Exciton efficiency beyond the spin statistical limit in organic light emitting diodes based on anthracene derivatives, J. Mater. Chem. C 8 (2020) 3773-3783.

[10] J. Zhang, Y. Zhao, H. Xu, D. Zhang, Y. Miao, R. Shinar, J. Shinar, H. Wang, B. Xu, Y. Wu, Novel blue fluorescent emitters structured by linking triphenylamine and

anthracene derivatives for organic light-emitting devices with EQE exceeding 5%, J. Mater. Chem. C 7 (2019) 10810-10817.

[11] Q. Liu, J. Guo, M. Fan, Q. Zhang, S. Liu, K.-L. Wong, Z. Liu, B. Wei, Fast synthesis of Dy^{3+} and Tm^{3+} co-doped double perovskite $NaLaMgWO_6$: A thermally stable single-phase white-emitting phosphor for WLEDs, J. Mater. Chem. C 8 (2020) 2117-2122.

[12] M.A. Baldo, D.F. O'Brien, Y. You, A. Shoustikov, S. Sibley, M.E. Thompson, S.R. Forrest, Highly efficient phosphorescent emission from organic electroluminescent devices, Nature 395 (1998) 151-154.

[13] W. Li, Y. Pan, R. Xiao, Q. Peng, S. Zhang, D. Ma, F. Li, F. Shen, Y. Wang, B. Yang, Y. Ma, Employing ~100% excitons in OLEDs by utilizing a fluorescent molecule with hybridized local and charge-transfer excited state, Adv. Funct. Mater. 24 (2014) 1609-1614.

[14] H. Liu, J. Li, W.-C. Chen, Z. Chen, Z. Liu, Q. Zhan, X. Cao, C.-S. Lee, C. Yang, Modulating the acceptor structure of dicyanopyridine based TADF emitters: Nearly 30% external quantum efficiency and suppression on efficiency roll-off in OLED, Chem. Eng. J. 401 (2020) 126107.

[15] T.-L. Wu, M.-J. Huang, C.-C. Lin, P.-Y. Huang, T.-Y. Chou, R.-W. Chen-Cheng, H.-W. Lin, R.-S. Liu, C.-H. Cheng, Diboron compound-based organic light-emitting diodes with high efficiency and reduced efficiency roll-off, Nat. Photonics 12 (2018) 235-240.

[16] Y. Xu, X. Liang, X. Zhou, P. Yuan, J. Zhou, C. Wang, B. Li, D. Hu, X. Qiao, X. Jiang, L. Liu, S.-J. Su, D. Ma, Y. Ma, Highly efficient blue fluorescent OLEDs based on upper level triplet-singlet intersystem crossing, Adv. Mater. 31 (2019) 1807388.

[17] L. Yao, S. Zhang, R. Wang, W. Li, F. Shen, B. Yang, Y. Ma, Highly efficient near-infrared organic light-emitting diode based on a butterfly-shaped donor-acceptor chromophore with strong solid-state fluorescence and a large proportion of radiative excitons, Angew. Chem. Int. Ed. 53 (2014) 2119-2123.

[18] Q. Zhang, B. Li, S. Huang, H. Nomura, H. Tanaka, C. Adachi, Efficient blue organic light-emitting diodes employing thermally activated delayed fluorescence, Nat.

Photonics 8 (2014) 326-332.
[19] Q. Zhang, J. Li, K. Shizu, S. Huang, S. Hirata, H. Miyazaki, C. Adachi, Design of efficient thermally activated delayed fluorescence materials for pure blue organic light emitting diodes, J. Am. Chem. Soc. 134 (2012) 14706-14709.
[20] Z. Zhang, D. Ding, Y. Wei, J. Zhang, C. Han, H. Xu, Excited-state engineering of universal ambipolar hosts for highly efficient blue phosphorescence and thermally activated delayed fluorescence organic light-emitting diodes, Chem. Eng. J. 382 (2020) 122485.
[21] J. Jayabharathi, V. Thanikachalam, S. Thilagavathy, J. Anudeebhana, Efficient m-shaped blue emitters having a high conjugation extent with improved roll-off efficiency, J. Mater. Chem. C 10 (2022) 11005-11015.
[22] Y. He, Z. Qiao, X. Cai, M. Li, W. Li, W. Xie, W. Qiu, L. Wang, S.-J. Su, Pyridine-based bipolar hosts for solution-processed bluish-green thermally activated delayed fluorescence devices: A subtle regulation of chemical stability and carrier transportation, ACS Appl. Mater. Interfaces 12 (2020) 49905-49914.
[23] J.-J. Zhu, Y. Chen, Y.-H. Xiao, X. Lian, G.-X. Yang, S.-S. Tang, D. Ma, Y. Wang, Q.-X. Tong, The structure optimization of phenanthroimidazole based isomers with external quantum efficiency approaching 7% in non-doped deep-blue OLEDs, J. Mater. Chem. C 8 (2020) 2975-2984.
[24] C. Lin, P. Han, S. Xiao, F. Qu, J. Yao, X. Qiao, D. Yang, Y. Dai, Q. Sun, D. Hu, A. Qin, Y. Ma, B.Z. Tang, D. Ma, Efficiency breakthrough of fluorescence OLEDs by the strategic management of “hot excitons” at highly lying excitation triplet energy levels, Adv. Funct. Mater. 31 (2021) 2106912.
[25] X. Lv, L. Xu, W. Cui, Y. Yu, H. Zhou, M. Cang, Q. Sun, Y. Pan, Y. Xu, D. Hu, S. Xue, W. Yang, High-efficiency, non-doped, pure-blue fluorescent organic light-emitting diodes via molecular tuning regulation of hot exciton excited states, ACS Appl. Mater. Interfaces 13 (2021) 970-980.
[26] Y. Zhang, C. Gao, P. Wang, Y. Liu, Z. Liu, W. Xie, H. Xu, Y. Dang, D. Liu, Z. Ren, S. Yan, Z. Wang, W. Hu, H. Dong, High electron mobility hot-exciton induced delayed fluorescent organic semiconductors, Angew. Chem. Int. Ed. 62 (2023) e202217653.

[27] Y. Pan, W. Li, S. Zhang, L. Yao, C. Gu, H. Xu, B. Yang, Y. Ma, High yields of singlet excitons in organic electroluminescence through two paths of cold and hot excitons, Adv. Opt. Mater. 2 (2014) 510-515.

[28] H. Zhang, B. Zhang, Y. Zhang, Z. Xu, H. Wu, P.-A. Yin, Z. Wang, Z. Zhao, D. Ma, B.Z. Tang, A multifunctional blue-emitting material designed via tuning distribution of hybridized excited-state for high-performance blue and host-sensitized OLEDs, Adv. Funct. Mater. 30 (2020) 2002323.

[29] W. Li, Y. Pan, L. Yao, H. Liu, S. Zhang, C. Wang, F. Shen, P. Lu, B. Yang, Y. Ma, A hybridized local and charge-transfer excited state for highly efficient fluorescent OLEDs: Molecular design, spectral character, and full exciton utilization, Adv. Opt. Mater. 2 (2014) 892-901.

[30] M. Pope, H.P. Kallmann, P. Magnante, Electroluminescence in organic crystals, J. Chem. Phys. 38 (1963) 2042-2043.

[31] F. Liu, Z. Cheng, L. Wan, L. Gao, Z. Yan, D. Hu, L. Ying, P. Lu, Y. Ma, Anthracene-based emitters for highly efficient deep blue organic light-emitting diodes with narrow emission spectrum, Chem. Eng. J. 426 (2021) 131351.

[32] S. Wang, M. Qiao, Z. Ye, D. Dou, M. Chen, Y. Peng, Y. Shi, X. Yang, L. Cui, J. Li, C. Li, B. Wei, W.-Y. Wong, Efficient deep-blue electrofluorescence with an external quantum efficiency beyond 10%, iScience 9 (2018) 532-541.

[33] Y. Zhu, S. Vela, H. Meng, C. Corminboeuf, M. Fumanal, Donor-acceptor-donor “hot exciton” triads for high reverse intersystem crossing in OLEDs, Adv. Opt. Mater. 10 (2022) 2200509.

[34] B. Liu, Z.W. Yu, D. He, M.D. Li, W.F. Xie, Q.X. Tong, Productive harvesting of triplet excitons in anthracene-based emitters toward high-performance deep-blue nondoped organic light-emitting diodes, Mater. Today Chem. 23 (2022) 100630.

[35] Y. Yu, P. Xu, Y. Pan, X. Qiao, L. Ying, D. Hu, D. Ma, Y. Ma, Pyrene-based emitters with ultrafast upper-level triplet-singlet intersystem crossing for high-efficiency, low roll-off blue organic light-emitting diode, Adv. Opt. Mater. 11 (2023) 2202217.

[36] X. Tang, Q. Bai, T. Shan, J. Li, Y. Gao, F. Liu, H. Liu, Q. Peng, B. Yang, F. Li, P. Lu, Efficient nondoped blue fluorescent organic light-emitting diodes (OLEDs) with a

high external quantum efficiency of 9.4% @ 1000 cd m^{-2} based on phenanthroimidazole-anthracene derivative, Adv. Funct. Mater. 28 (2018) 1705813.
[37] Y. Xu, C. Wang, X. Zhou, J. Zhou, X. Guo, X. Liang, D. Hu, F. Li, D. Ma, Y. Ma, Fine modulation of the higher-order excitonic states toward more efficient conversion from upper-level triplet to singlet, J. Phys. Chem. Lett 10 (2019) 6878-6884.
[38] C. Lin, P. Han, F. Qu, S. Xiao, Y. Li, D. Xie, X. Qiao, D. Yang, Y. Dai, Q. Sun, A. Qin, B.Z. Tang, D. Ma, Suppressing singlet-triplet annihilation processes to achieve highly efficient deep-blue AIE-based OLEDs, Mater. Horizons 9 (2022) 2376-2383.
[39] J.-Y. Hu, Y.-J. Pu, F. Satoh, S. Kawata, H. Katagiri, H. Sasabe, J. Kido, Bisanthracene-based donor-acceptor-type light-emitting dopants: Highly efficient deep-blue emission in organic light-emitting devices, Adv. Funct. Mater. 24 (2014) 2064-2071.
[40] L. Xing, Z.-L. Zhu, J. He, Z. Qiu, Z. Yang, D. Lin, W.-C. Chen, Q. Yang, S. Ji, Y. Huo, C.-S. Lee, Anthracene-based fluorescent emitters toward superior-efficiency nondoped TTA-OLEDs with deep blue emission and low efficiency roll-off, Chem. Eng. J. 421 (2021) 127748.